12th International Symposium on Turbulence and Shear Flow Phenomena (TSFP12)
Osaka, Japan (Online), July 19-22, 2022

STABILITY AND RESOLVENT ANALYSIS OF PLANE COUETTE FLOW IN THE DISTINGUISHED LIMIT $Re \to \infty, \alpha \to 0$ WITH $Re \cdot \alpha = O(1)$

Toni Dokoza
Chair of Fluid Dynamics, Department of Mechanical Engineering
Technical University of Darmstadt
64287 Darmstadt, Germany
dokoza@fdy.tu-darmstadt.de

Martin Oberlack
Chair of Fluid Dynamics, Department of Mechanical Engineering
Technical University of Darmstadt
64287 Darmstadt, Germany
oberlack@fdy.tu-darmstadt.de

ABSTRACT

In this work the plane Couette flow is being investigated for high Reynolds numbers $Re \to \infty$ and small streamwise wavenumbers $\alpha \to 0$ in the distinguished limit $Re_\alpha = Re\alpha = O(1)$ using the temporal linear stability theory as well as the resolvent analysis approach. The influence of Re_α on both the eigenfunctions obtained from the linear stability theory and the repsonse modes obtained from the resolvent analysis is investigated, while both modes are being compared in order to analyse the occurence of streamwise-elongated coherent structures within the plane Couette flow.

INTRODUCTION

It is well known that for a high enough Reynolds number Re the plane Couette flow becomes turbulent and thus both small- and large-scale structures are observed. In order to investigate the large streamwise-elongated structures, which can be observed in plane Couette flow, the linear analysis of the Navier–Stokes equations in shear flows (Schmid & Henningson, 2001) provide useful insights. These linear analyses reveal that, for the plane Couette flow, the structures that are most excitable are streamwise-constant. The observation of streamwise-constant structures being most amplified has been made for the laminar plane Couette flow among many others by Gustavsson (1981) for example, as well as for its turbulent counterpart for which the linear analyses are performed about the turbulent mean flow in Hwang & Cossu (2010*a*). In turbulent flows, coherent structures can be understood as being permanently forced via convective nonlinear interactions of the fluctuations. Thus it seems appropriate to analyse the flow behaviour as the response to a non-linear intrinsic forcing through a linearised operator, which is the key idea of the resolvent analysis, where all the non-linear fluctuation terms in the Navier-Stokes equations for the perturbations are summarised as an intrinsic forcing term $f_i' = -u_j' \frac{\partial u_i'}{\partial x_j}$, through which the Navier-Stokes equation can be rewritten in an input-output system. A singular-value-decomposition (SVD) is being performed in order to rewrite the resolvent operator in the most amplified response modes and their associated forcing modes, which are coupled by the singular values. This work aims to investigate the coherent structures through both the resolvent analysis and the linear stability theory with a laminar base velocity profile for the limit of high Reynolds numbers $Re \to \infty$ and simultaneously small streamwise wavenumbers $\alpha \to 0$ with the distinguished limit $Re_\alpha = Re\alpha = O(1)$.

GOVERNING EQUATIONS

The Navier-Stokes equations for the velocity fluctuations u_i' around a laminar base veloctiy profile in streamwise direction x_1, given by $U_1(x_2) = x_2$ are given in wall-normal velocity-vorticity formulation of the plane Couette flow for the wall-normal velocity fluctuation u_2' and the wall-normal vorticity fluctuation $\eta_2' = \frac{\partial u_1'}{\partial x_3} - \frac{\partial u_3'}{\partial x_1}$. Hereby spatial directions are represented by x_i with $i = 1,2,3$. Solid wall boundary conditions for the wall-normal velocity-vorticity formulation are Dirichlet boundary conditions for u_2' and η_2' as well as the Neumann boundary condition for u_2', i.e. $\left(u_2',\ \frac{\partial u_2'}{\partial x_2},\ \eta_2'\right)^\mathsf{T}(x_1, x_2 = \pm 1, x_3) = 0$. A Fourier decomposition in streamwise and spanwise direction as well as in time is applied using

$$u_i' = \tilde{u}_i'(x_2) e^{\mathrm{i}(\alpha x_1 + \beta x_3 - \omega t)}, \tag{1}$$

$$\eta_2' = \tilde{\eta}_2'(x_2) e^{\mathrm{i}(\alpha x_1 + \beta x_3 - \omega t)}, \tag{2}$$

with α an β being the streamwise and spanwise wavenumber, while ω represents the frequency of the fluctuations, which leads to the governing equations as

$$\begin{aligned} &-\mathrm{i}\omega\left((\alpha^2+\beta^2)\tilde{u}_2' - \frac{d^2\tilde{u}_2'}{dx_2^2}\right) + \mathrm{i}\alpha x_2\left((\alpha^2+\beta^2)\tilde{u}_2' - \frac{d^2\tilde{u}_2'}{dx_2^2}\right) \\ &\quad + \frac{1}{Re}\left(\frac{d^4\tilde{u}_2'}{dx_2^4} - 2(\alpha^2+\beta^2)\frac{d\tilde{u}_2'}{dx_2^2} + (\alpha^2+\beta^2)^2\tilde{u}_2'\right) \\ &\quad = -\mathrm{i}\alpha\frac{d\tilde{f}_1'}{dx_2} - \beta^2\tilde{f}_2' - \mathrm{i}\beta\frac{d\tilde{f}_3'}{dx_2}, \end{aligned} \tag{3}$$

$$-\mathrm{i}\omega\tilde{\eta}_2' + x_2\mathrm{i}\alpha\tilde{\eta}_2' + \mathrm{i}\beta\tilde{u}_2' + \frac{1}{Re}\left(-\frac{\partial^2\eta_2'}{\partial x_2^2} + (\alpha^2+\beta^2)\tilde{\eta}_2'\right) = \mathrm{i}\beta\tilde{f}_1' - \mathrm{i}\alpha\tilde{f}_3' \quad (4)$$

and

$$\mathrm{i}\alpha\tilde{u}_1' + \frac{d\tilde{u}_2'}{dx_2} + \mathrm{i}\beta\tilde{u}_3' = 0, \quad (5)$$

with the Reynoldsnumber Re, where $\tilde{f}_i = \left(-u_j'\frac{\partial u_i'}{\partial x_j}\right)_{\mathbf{k}}$ denotes the Fourier-transformed nonlinear forcing term corresponding to the wavenumber vector $\mathbf{k} = (\alpha,\ \beta,\ \omega)^\mathsf{T}$. We are presently particularly interested in large-scale coherent structures which are observed to occur for high Reynolds number flows and which admit very weak streamwise variation, since these are structures found to be most amplified (Hwang & Cossu (2010*b*)). Hence, we intend to analyse the distinguished asymptotic limit of $\alpha \to 0$ and $Re \to \infty$, which are the key parameters to observe coherent structures in the form of counter rotating vortices occupying the whole channel width. Thus we introduce $Re_\alpha = Re\cdot\alpha$, which is to be considered of order $O(1)$, as done in Yalcin *et al.* (2021) for the temporal linear stability of the asymptotic suction boundary layer. We may neglect all terms of order $\mathrm{O}(\alpha^n)$ with $n > 1$ in the equation (3) and the equation (4), leading to

$$-\mathrm{i}\frac{\omega}{\alpha}Re_\alpha\left(\beta^2\tilde{u}_2' - \frac{d^2\tilde{u}_2'}{dx_2^2}\right) + \mathrm{i}Re_\alpha\left(x_2\beta^2\tilde{u}_2' - \frac{d^2\tilde{u}_2'}{dx_2^2}\right) + \frac{d^4\tilde{u}_2'}{dx_2^4} - 2\beta^2\frac{d^2\tilde{u}_2'}{dx_2^2} + \beta^4\tilde{u}_2' = \frac{Re_\alpha}{\alpha}\left(-\mathrm{i}\alpha\frac{d\tilde{f}_1'}{dx_2} - \beta^2\tilde{f}_2' - \mathrm{i}\beta\frac{d\tilde{f}_3'}{dx_2}\right) \quad (6)$$

and

$$-\mathrm{i}\frac{\omega}{\alpha}Re_\alpha\tilde{\eta}_2' + x_2\mathrm{i}Re_\alpha\tilde{\eta}_2' + \frac{Re_\alpha}{\alpha}\mathrm{i}\beta\tilde{u}_2' - \frac{d^2\tilde{\eta}_2'}{dx_2^2} + \beta^2\tilde{\eta}_2' = \frac{Re_\alpha}{\alpha}(\mathrm{i}\beta\tilde{f}_1' - \mathrm{i}\alpha\tilde{f}_3'). \quad (7)$$

RESOLVENT ANALYSIS

For the resolvent analysis it is necessary to rewrite the partial differential equations (3) and (4) in an input-output system as

$$-\mathrm{i}\omega\mathbf{M}\tilde{\mathbf{q}}' = \mathbf{L}\tilde{\mathbf{q}}' + \mathbf{B}\tilde{\mathbf{f}}', \quad (8)$$

with $\tilde{\mathbf{q}}' = \begin{pmatrix}\tilde{u}_2'\\ \tilde{\eta}_2'\end{pmatrix}$ and $\tilde{\mathbf{f}}' = \begin{pmatrix}\tilde{f}_1'\\ \tilde{f}_2'\\ \tilde{f}_3'\end{pmatrix}$.
Hereby the mass-matrix $\mathbf{M}$ reads

$$\mathbf{M} = \begin{pmatrix}\frac{Re_\alpha}{\alpha}\left(\frac{d^2}{dx_2^2} - \beta^2\right) & 0\\ 0 & \frac{Re_\alpha}{\alpha}\end{pmatrix}, \quad (9)$$

with $\mathbf{L}$, representing the Orr-Sommerfeld and Squire operator, is given as

$$\mathbf{L} = \begin{pmatrix}L_{11} & 0\\ L_{21} & L_{22}\end{pmatrix}, \quad (10)$$

with

$$L_{11} = -x_2\mathrm{i}Re_\alpha\left(\frac{d^2}{dx_2^2} - \beta^2\right) + \frac{d^4}{dx_2^4} - 2\beta^2\frac{d^2}{dx_2^2} + \beta^4$$
$$L_{21} = -\frac{Re_\alpha}{\alpha}\mathrm{i}\beta$$
$$L_{22} = -x_2\mathrm{i}Re_\alpha + \frac{d^2}{dx_2^2} - \beta^2 \quad (11)$$

and the matrix $\mathbf{B}$ is given as

$$\mathbf{B} = \begin{pmatrix}-\mathrm{i}Re_\alpha\frac{d}{dx_2} & -\frac{Re_\alpha}{\alpha}\beta^2 & -\mathrm{i}\beta\frac{Re_\alpha}{\alpha}\frac{d}{dx_2}\\ \frac{Re_\alpha}{\alpha}\mathrm{i}\beta & 0 & -\frac{Re_\alpha}{\alpha}\mathrm{i}\alpha\end{pmatrix}. \quad (12)$$

All velocity fluctuations $\tilde{u}_i'$ are generated from $\tilde{u}_2'$ and $\tilde{\eta}_2'$ using the continuity equation (5), since u_2' and η_2' are considered as known quantities. The veloctiy fluctuations u_i' are then given by

$$\begin{pmatrix}\tilde{u}_1'\\ \tilde{u}_2'\\ \tilde{u}_3'\end{pmatrix} = \mathbf{C}\begin{pmatrix}\tilde{u}_2'\\ \tilde{\eta}_2'\end{pmatrix} = \frac{1}{\beta^2}\begin{pmatrix}\mathrm{i}\alpha\frac{d}{dx_2} & -\mathrm{i}\beta\\ \beta^2 & 0\\ \mathrm{i}\beta\frac{d}{dx_2} & \mathrm{i}\alpha\end{pmatrix}. \quad (13)$$

In a final step we may rewrite (8) by introducing the resolvent matrix $\mathbf{H}$ as

$$\tilde{\mathbf{q}}' = \mathbf{H}\tilde{\mathbf{f}}_B' = (-\mathbf{L} - \mathrm{i}\omega_1\mathbf{M})^{-1}\tilde{\mathbf{f}}_B'. \quad (14)$$

Singular Value Decomposition

The goal of the resolvent analysis is to identify the dominant directions along which $\tilde{\mathbf{f}}_B'$ can be most amplified through the resolvent operator $\mathbf{H}$ to form the corresponding responses in $\tilde{\mathbf{q}}'$. By using a singular value decomposition on the resolvent operator $\mathbf{H}$ one can obtain these modes. The response modes are considered to represent the occurring coherent structures, observed in plane Couette flow, where only the knowledge of the mean velocity profile has to be taken from external sources. The singular value decomposition rewrites the matrix $\mathbf{H}$ into

$$\mathbf{H} = \mathbf{USV}^T = \begin{pmatrix}| & | & & |\\ \Psi_1 & \Psi_2 & \dots & \Psi_n\\ | & | & & |\end{pmatrix}\begin{pmatrix}\sigma_1 & & \\ & \ddots & \\ & & \sigma_n\end{pmatrix}\begin{pmatrix}- & \Phi_1 & -\\ & \dots & \\ - & \Phi_n & -\end{pmatrix}.$$

In this formulation $\mathbf{S}$ represents a diagonal matrix with the singular values σ_n in decreasing order in its diagonal. The matrix $\mathbf{V}^T$ contains the forcing modes $\vec{\Phi}_j$, while $\mathbf{U}$ contains the respective response modes $\vec{\Psi}_j$. Both sets of singular vectors are guaranteed to be orthonormal bases and are ranked according to their singular values. In other words, the resolvent analysis interprets left and right singular vectors $\tilde{\mathbf{q}}'$ and $\tilde{\mathbf{f}}_B'$ of $\tilde{\mathbf{q}}' = \mathbf{H}\tilde{\mathbf{f}}_B'$ respectively as response and forcing modes, with the magnitude-ranked singular values σ_i being the amplification (gain) for the corresponding forcing-response pair. The resolvent operator is of lower rank if $\sum_{j=1}^{p}\sigma_j^2 \approx \sum_{j=1}^{\infty}\sigma_j^2$, where $\sigma_p \gg \sigma_{p+1}$ and the number of these singular values p is small. If the resolvent operator is rank-1, hence $\sigma_1 \gg \sigma_2$, the response can be well predicted from the leading singular vectors alone.

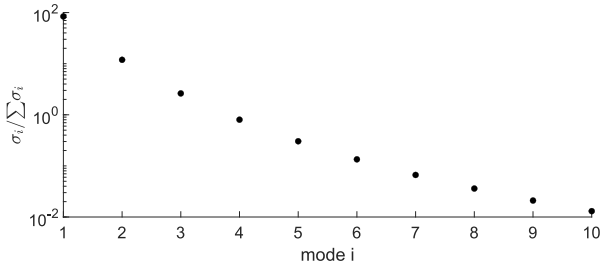

Figure 1. Share of first 10 singular values of the resolvent operator over all singular values for $\omega = 0$, $\beta = 2$, $Re_\alpha = 1$, $\alpha = 0.0001$.

Numerical methods and discretisation

The input-output system (14) is being analysed numerically using Matlab. The matrix system (14) is discretised in wall-normal direction x_2 using a Chebyshev-discretisation with $N = 251$ collocation points, whereas the differentiation matrices are being built using the chebdif function by Weideman & Reddy (2000). The Dirichlet boundary and Neumann boundary conditions for the wall-normal velocity u_2' and the Dirichlet boundary condition for the wall-normal vorticity η_2' are implemented using the cheb4c function by Weideman & Reddy (2000). The resolvent operator is scaled to the kinetic energy for wall-normal fluctuations as described in Schmid & Henningson (2001) as

$$E_v = \int_\alpha \int_\beta \frac{1}{2k^2} \int_{-1}^{1} \left(\left| \frac{\partial}{\partial x_2} u_2' \right|^2 + k^2 |u_2'|^2 + |\eta_2'|^2 \right) dy d\alpha d\beta, \tag{15}$$

with $k = \alpha^2 + \beta^2$.

Results

Figure 1 shows the share of the first 10 singular values over all singular values for $\omega = 0$, $\beta = 2$, $Re_\alpha = 1$ and $\alpha = 0.0001$. The share of each singular value decreases over-exponentially with increasing modes. One can see that σ_1 makes up to 82 % of all singular values, thus a low-rank behaviour can be assumed, allowing the coherent structures to be well estimated by only using the first response modes in the subsequent investigations. In Figure 2 the forcing modes are shown over the wall-normal direction x_2 on the left and the corresponding response modes on the right side for $\omega = 0$, $\beta = 2$, $Re_\alpha = 1$, $\alpha = 0.0001$. It can be seen that the most energy can be found in the streamwise fluctuation u_1' for the considered distinguished limit. The magnitude of the wall-normal and spanwise fluctuations are of order $O(\alpha)$ compared to the streamwise fluctuation, thus the streamwise streaks can be observed. Furthermore, we observe, that the energy within the forcing is mainly given in the wall-normal and spanwise components, while the energy of the response is stored in the streamwise component. Spanwise and wall-normal forcing modes give rise to streamwise response modes, indicating the lift-up effect being dominant.

The first response modes $\tilde{u}_1'$, $\tilde{u}_2'$, $\tilde{u}_3'$ for $\omega = 0, \beta = 2, Re_\alpha = 1, \alpha = 0.0001$ are shown over the wall-normal direction x_2 in Figure 3. It once agains shows the most energy being stored in the streamwise direction.

Figure 4 shows the response of the system as streamwise fluctuations over the the spanwise and wall-normal direction for a variation of α on the left side with a fixed Re and for various Re on the right side for a fixed α, where Re_α on each

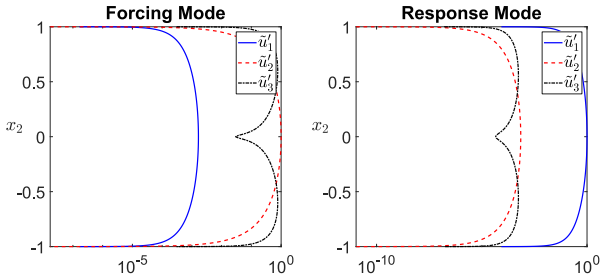

Figure 2. Forcing modes and Response modes for each velocity fluctuation for $\omega = 0$, $\beta = 2$, $Re_\alpha = 1$, $\alpha = 0.0001$ are shown over the wall-normal coordinate x_2.

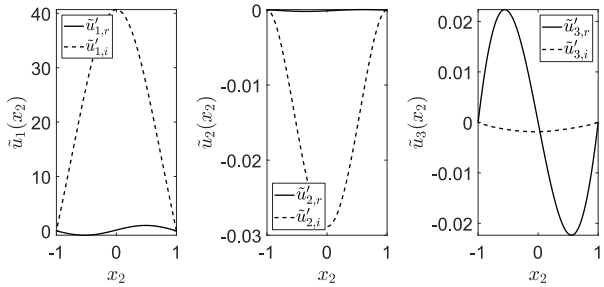

Figure 3. First response modes $\tilde{u}_1'$, $\tilde{u}_2'$, $\tilde{u}_3'$ for $\omega = 0, \beta = 2, Re_\alpha = 1, \alpha = 0.0001$ are shown over the wall-normal direction x_2. Solid lines represent the real part of the solution, with dotted lines representing the imaginary part of the response modes.

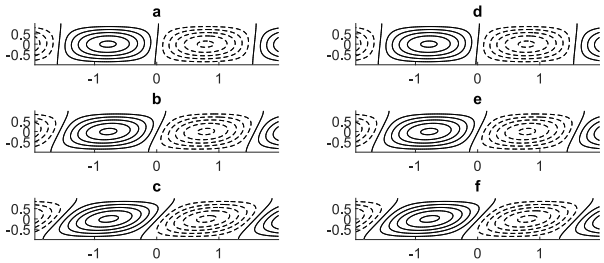

Figure 4. Streamwise fluctuations are shown over the spanwise direction x_3 and wall-normal direction x_2 for (a) $\omega = 0$, $\beta = 2$, $Re_\alpha = 1$, $\alpha = 0.0001$, (b) $\omega = 0$, $\beta = 2$, $Re_\alpha = 5$, $\alpha = 0.0005$, (c) $\omega = 0, \beta = 2, Re_\alpha = 10, \alpha = 0.001$, (d) $\omega = 0$, $\beta = 2$, $Re_\alpha = 1$, $Re = 10000$, (e) $\omega = 0$, $\beta = 2$, $Re_\alpha = 5$, $Re = 50000$, (f) $\omega = 0$, $\beta = 2$, $Re_\alpha = 10$, $Re = 100000$, as pairs of vortices. Solid lines represent fluctuations with a positive sign, while dashed lines represent fluctuations with a negative sign.

row is equal on both the left and the right side. One can see that an increase of Re_α leads to a stronger inclination of the streamwise structures within the spanwise and wall-normal direction, while the effect of an increasing Re and an increasing α is the same, which can be seen through the fact that the coherent structures in (a) and (d), (b) and (e), (c) and (f) are the same. Thus Re_α effects the inclination of these strucutures rather than α or Re alone. The Orr-mechansim yields an inclination of the structures in the direction of the propagating waves. Since for $\alpha \neq 0$, the waves are not propagating in the streamwise direction alone anymore, an inclination within the spanwise and wall-normal direction can be observed. The influence of β and Re_α on σ_1 and thus the energy of the system for $\omega = 0$ is now being investigated. For this purpose Figure

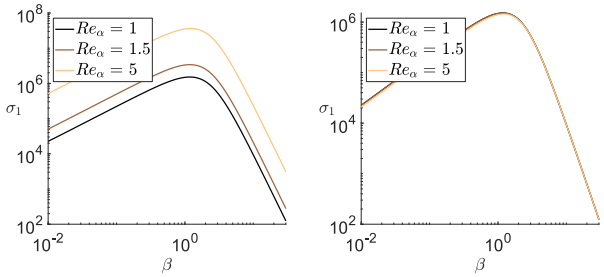

Figure 5. The first singular value σ_1 is shown over β for $\omega = 0$ for a fixed $\alpha = 0.0001$ and three different values for Re on the left side and for a fixed $Re = 10000$ and three different values for α on the right side.

5 shows the behaviour of σ_1 over β for three different values of Re_α for a fixed $\alpha = 0.0001$ and three different values of Re on the left side and for a fixed $Re = 10000$ and three different values for α on the right side. It can be seen that σ_1 first increases with β^1 for an increasing β before declining with β^{-2} after reaching its peak. On the left hand side Re_α is increased by setting $\alpha = 0.0001$ and increasing Re. It can be seen that σ_1 increases with increasing Re_α for a fixed α. On the right side the Reynolds number was set to $Re = 10000$, while α is being changed. Increasing Re_α on this way, leads to a decreasing first singular value, agreeing with the findings of Hwang & Cossu (2010*a*) that streamwise-constant structures are being most amplified.

LINEAR STABILITY THEORY

In this section we want to investigate the distinguished asymptotic limit with $Re_\alpha = O(1)$ for the plane Couette flow using the linear stability theory, where the Orr-Sommerfeld and the Squire equation are obtained by setting the right-hand side of (6) and (7) to 0 due to considering only small fluctuations. Furthermore we observe that in these equations terms of the order $\frac{\omega}{\alpha}$ prevail, and hence, a low frequency assumption is implied with $\omega = \omega_1\alpha + O(\alpha^2)$, leading to the expanded Orr-Sommerfeld and Squire equation given as

$$-\mathrm{i}\omega_1 Re_\alpha\left(\beta^2\tilde{u}_2' - \frac{d^2\tilde{u}_2'}{dx_2^2}\right) + \mathrm{i}Re_\alpha x_2\beta^2\tilde{u}_2' - \mathrm{i}Re_\alpha x_2\frac{d^2\tilde{u}_2'}{dx_2^2} + \frac{d^4\tilde{u}_2'}{dx_2^4} - 2\beta^2\frac{d^2\tilde{u}_2'}{dx_2^2} + \beta^4\tilde{u}_2' = 0 \tag{16}$$

and

$$-\mathrm{i}\omega_1 Re_\alpha\tilde{\eta}_2' + x_2\mathrm{i}Re_\alpha\tilde{\eta}_2' + \frac{Re_\alpha}{\alpha}\mathrm{i}\beta\tilde{u}_2' - \frac{d^2\tilde{\eta}_2'}{dx_2^2} + \beta^2\tilde{\eta}_2' = 0. \tag{17}$$

The Orr-Sommerfeld equation (16) is only dependent on the newly introduced variable Re_α, whereas the Squire-equation (17) still contains α. Thus the wall-normal velocity fluctuation $\tilde{u}_2'$ has to be of order $O(\alpha)$ compared to the wall-normal vorticity fluctuation $\tilde{\eta}_2'$ in order for all the terms to be of the same order.

Therefore, we rewrite the wall-normal velocity fluctuation as $\tilde{u}_2 = \alpha\tilde{u}_{2,\alpha}$, where α is used to rescale $\tilde{u}_2$. By this assumption α formally vanishes in the Squire equation (17) as well, leading to the further expanded Orr-Sommerfeld and Squire operators

$$-\mathrm{i}\omega_1 Re_\alpha\left(\beta^2\tilde{u}_{2,\alpha}' - \frac{d^2\tilde{u}_{2,\alpha}'}{dx_2^2}\right) + \mathrm{i}Re_\alpha x_2\beta^2\tilde{u}_{2,\alpha}' - \mathrm{i}Re_\alpha x_2\frac{d^2\tilde{u}_{2,\alpha}'}{dx_2^2} + \frac{d^4\tilde{u}_{2,\alpha}'}{dx_2^4} - 2\beta^2\frac{d^2\tilde{u}_{2,\alpha}'}{dx_2^2} + \beta^4\tilde{u}_{2,\alpha}' = 0 \tag{18}$$

and

$$-\mathrm{i}\omega_1 Re_\alpha\tilde{\eta}_2' + x_2\mathrm{i}Re_\alpha\tilde{\eta}_2' + Re_\alpha\mathrm{i}\beta\tilde{u}_{2,\alpha}' - \frac{d^2\tilde{\eta}_2'}{dx_2^2} + \beta^2\tilde{\eta}_2' = 0. \tag{19}$$

The solution for $\tilde{u}_{2,\alpha}'$ is obtained analytically from the Orr-Sommerfeld equation (18) in terms of Airy-functions $\mathrm{Ai}(z)$ and $\mathrm{Bi}(z)$ as

$$\begin{aligned}\tilde{u}_{2,\alpha}' = {} & \mathrm{C}_1 e^{\beta x_2} + \mathrm{C}_2 e^{\beta x_2}\int_{-1}^{x_2} e^{-2\beta x_2}dx_2 \\ & + \mathrm{C}_3\left(\frac{e^{\beta x_2}}{2\beta}E_1(Re_\alpha,\beta,\omega_1,x_2) - \frac{e^{-\beta x_2}}{2\beta}E_2(Re_\alpha,\beta,\omega_1,x_2)\right) \\ & + \mathrm{C}_4\left(\frac{e^{\beta x_2}}{2\beta}E_3(Re_\alpha,\beta,\omega_1,x_2) - \frac{e^{-\beta x_2}}{2\beta}E_4(Re_\alpha,\beta,\omega_1,x_2)\right),\end{aligned} \tag{20}$$

with

$$E_j(Re_\alpha,\beta,\omega_1,x_2) = \int_{-1}^{x_2} e^{(-1)^j\beta x_2} \cdot \mathrm{Ai}\left((-i)^{1/3}Re_\alpha^{-2/3}(Re_\alpha(\omega_1 - x_2) + i\beta^2)\right)dx_2, \tag{21a}$$

with $j = 1,2$ and

$$E_l(Re_\alpha,\beta,\omega_1,x_2) = \int_{-1}^{x_2} e^{(-1)^l\beta x_2} \cdot \mathrm{Bi}\left((-i)^{1/3}Re_\alpha^{-2/3}(Re_\alpha(\omega_1 - x_2) + i\beta^2)\right)dx_2, \tag{21b}$$

with $l = 3,4$. The eigenvalues ω_1 are being solved from the eigenvalue problem using the Orr-Sommerfeld equation (18) based on a Matlab Chebyshev collocation code as done in Schmid & Henningson (2001) with the boundary conditions $\left(u_2', \frac{\partial u_2'}{\partial x_2}\right)^\mathsf{T}(x_1, x_2 = \pm 1, x_3) = 0$, which may be written in matrix form as

$$\mathbf{A}(Re_\alpha,\beta,\omega_1)\cdot\begin{pmatrix}C_1\\C_2\\C_3\\C_4\end{pmatrix} = \begin{pmatrix}A_{11} & A_{12} & A_{13} & A_{14}\\ A_{21} & 0 & 0 & 0\\ A_{31} & A_{32} & A_{33} & A_{34}\\ A_{41} & A_{42} & 0 & 0\end{pmatrix}\cdot\begin{pmatrix}C_1\\C_2\\C_3\\C_4\end{pmatrix}. \tag{22}$$

A_{ij} represent the respective coefficients for the boundary conditions $\left(u_2', \frac{\partial u_2'}{\partial x_2}\right)^\mathsf{T}(x_1, x_2 = \pm 1, x_3) = 0$. For a non-trivial solution the determinant of $\mathbf{A}$ has to vanish, yielding the dispersion relation

$$\det(\mathbf{A}(Re_\alpha,\beta,\omega_1)) = A_{14}A_{33} - A_{13}A_{34} = 0, \tag{23}$$

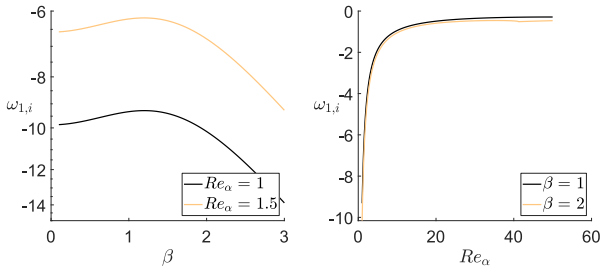

Figure 6. Most critical numerically obtained eigenvalue $\omega_{1,\mathrm{i}}$ is plotted over β for $Re_\alpha = [1, 1.5]$ on the left side and plotted over Re_α for $\beta = [1, 2]$ on the right side.

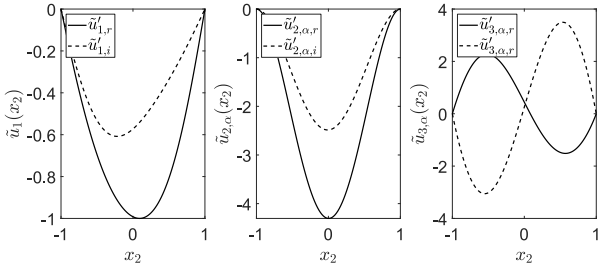

Figure 7. Analytically obtained eigenfunctions $\tilde{u}'_1, \tilde{u}'_{2,\alpha}, \tilde{u}'_{3,\alpha}$ for $\beta = 2, Re_\alpha = 1$ and for the most critical eigenvalue $\omega_1 = -10.1588\mathrm{i}$ are shown over the wall-normal direction x_2. Solid lines represent the real part of the solution, with dotted lines representing the imaginary part of the eigenfunctions.

from which the eigenvalues are obtained numerically. It is noticeable that using the linear stability theory the problem is only dependent of Re_α instead of an additional α, which was the case for the resolvent analysis. In Figure 6 the most critical numerically obtained eigenvalue $\omega_{1,\mathrm{i}}$ is shown over β for $Re_\alpha = [1, 1.5]$ on the left side and plotted over Re_α for $\beta = [1, 2]$ on the right side. It can be seen that the most critical numerically obtained eigenvalue $\omega_{1,\mathrm{i}}$ over β follows a similar qualitative behaviour as the first singular value σ_1 shown in Figure 5. For larger values of Re_α the most critical numerical eigenvalue $\omega_{1,\mathrm{i}}$ converges towards a value close to 0.
In order to solve for the coefficients C_i in (20), first the Dirichlet and Neumann boundary condition for the lower wall at $x_2 = -1$ is being implemented, leading to

$$\tilde{u}'_{2,\alpha}(x_2 = -1) = \mathrm{C}_1 e^{-\beta} = 0, \tag{24}$$

$$\frac{\partial \tilde{u}'_{2,\alpha}}{\partial x_2}(x_2 = -1) = \beta \mathrm{C}_1 e^{-\beta} + \mathrm{C}_2 e^{\beta} = 0, \tag{25}$$

so that $\mathrm{C}_1 = \mathrm{C}_2 = 0$. The Dirchlet boundary condition for the upper wall at $x_2 = 1$ then leads to

$$\mathrm{C}_3 = \frac{e^{-\beta} E_4(Re_\alpha, \beta, \omega_1, 1) - e^{\beta} E_3(Re_\alpha, \beta, \omega_1, 1)}{e^{\beta} E_1(Re_\alpha, \beta, \omega_1, 1) - e^{-\beta} E_2(Re_\alpha, \beta, \omega_1, 1)} \mathrm{C}_4. \tag{26}$$

In order to solve for the wall-normal vorticity $\tilde{\eta}'_2$ analytically, the Squire equation (19) can be used, resulting in

$$\begin{aligned} \tilde{\eta}'_2 &= \mathrm{C}_5 \mathrm{Ai}\left(Z(x_2)\right) + \mathrm{C}_6 \mathrm{Bi}\left(Z(x_2)\right) \\ &+ \frac{iA\pi\beta Re_\alpha}{(-iRe_\alpha)^{1/3}} \left[\mathrm{Ai}\left(Z(x_2)\right) \cdot \int_{-1}^{1} \mathrm{Bi}\left(Z(x_2)\right) \tilde{u}'_{2,\alpha} dx_2 \right. \\ &\left. - \mathrm{Bi}\left(Z(x_2)\right) \int_{-1}^{1} \mathrm{Ai}\left(Z(x_2)\right) \tilde{u}'_{2,\alpha} dx_2 \right], \end{aligned} \tag{27}$$

with $Z(x_2) = (-i)^{1/3} Re_\alpha^{-2/3} (Re_\alpha (\omega_1 - x_2) + i\beta^2)$. First the Dirichlet boundary condition for the lower wall at $x_2 = -1$ for $\tilde{\eta}'_2$ is being implemented, leading to

$$\mathrm{C}_5 = -\frac{\mathrm{Bi}\left(Z(x_2 = -1)\right)}{\mathrm{Ai}\left(Z(x_2 = -1)\right)} \mathrm{C}_6 = -\gamma \mathrm{C}_6. \tag{28}$$

Finally the boundary condition for the upperwall at $x_2 = 1$ for $\tilde{\eta}'_2$ is being implemented, resulting in

$$\begin{aligned} \mathrm{C}_6 = & \\ &- \mathrm{C}_4 \frac{\mathrm{i}\pi\beta Re_\alpha}{(-\mathrm{i}Re_\alpha)^{1/3}} \left[\kappa \mathrm{Ai}\left(Z(x_2 = 1)\right) \int_{-1}^{1} \mathrm{Bi}(Z(x_2)) \tilde{u}'_{2,\alpha} dx_2 \right. \\ &\left. - \kappa \mathrm{Bi}\left(Z(x_2 = 1)\right) \int_{-1}^{1} \mathrm{Ai}\left(Z(x_2)\right) \tilde{u}'_{2,\alpha} dx_2 \right], \end{aligned} \tag{29}$$

with $\frac{1}{\kappa} = -\gamma \mathrm{Bi}\left(Z(x_2 = 1)\right) + \mathrm{Ai}\left(Z(x_2 = 1)\right)$. The streamwise and spanwise fluctuations $\tilde{u}'_1, \tilde{u}'_3$ can be obtained using the coninuity equation (5), resulting in

$$\tilde{u}'_1 = -\frac{\mathrm{i}}{\beta} \tilde{\eta}'_2, \tag{30a}$$

$$\tilde{u}'_3 = \frac{\mathrm{i}}{\beta} \alpha \tilde{u}'_{2,\alpha} + \frac{\mathrm{i}}{\beta} \alpha \tilde{\eta}'_2. \tag{30b}$$

Inserting (20) in $\tilde{u}'_2 = \alpha \tilde{u}_{2,\alpha}$ one can see that α acts as a magnitude amplifier in the wall-normal fluctuation $\tilde{u}'_2$, while its qualitative behaviour is only dependent of Re_α. From (27) it can be seen that the wall-normal vorticity fluctuation is only dependent of Re_α in both its qualitative and quantitative behaviour. From (30a) one can see that the streamwise velocity fluctuation $\tilde{u}'_1$ is only dependent of the wall-normal vorticity fluctuation η'_2, thus also only dependent of Re_α. Furthermore one can see in (30b) that one could rewrite $\tilde{u}'_3 = \alpha \tilde{u}'_{3,\alpha}$, with $\tilde{u}'_{3,\alpha} = \frac{\mathrm{i}}{\beta} \tilde{u}'_{2,\alpha} + \frac{\mathrm{i}}{\beta} \tilde{\eta}'_2$, thus α would also only acts as a magnitude amplifier for $\tilde{u}'_3$, while its qualitative behaviour is only dependent of Re_α.
Figure 7 shows the analytically obtained eigenfunctions for the re-scaled wall-normal velocity fluctuation $\tilde{u}_{2,\alpha}$ as solved for in (20), where the wall-normal vorticity fluctuation $\tilde{\eta}'_2$ together with (30) was used in order to obtain the streamwise velocity fluctuation $\tilde{u}'_1$ and the re-scaled spanwise velocity fluctuation $\tilde{u}'_{3,\alpha}$ for $\beta = 1, Re_\alpha = 1$ and the most critical eigenvalue being found numerically using (23) found at $\omega_1 = -10.1588\mathrm{i}$. In Figure 8 the streamwise velocity fluctuation is shown over the spanwise and wall-normal direction for (a) $\beta = 2$, $Re_\alpha = 1$, $\omega_1 = -10.1588\mathrm{i}$, (b) $\beta = 2$, $Re_\alpha = 5$, $\omega_1 = -2.0508\mathrm{i}$ and (c) $\beta = 2$, $Re_\alpha = 10$, $\omega_1 = -1.0522\mathrm{i}$ as pairs of vortices. It can be seen that an increasing value of Re_α causes a stronger inclination of these vortices in the wall-normal and spanwise plane, while the influence of Re_α on the inclination is stronger then for the resolvent modes shown in Figure 4.

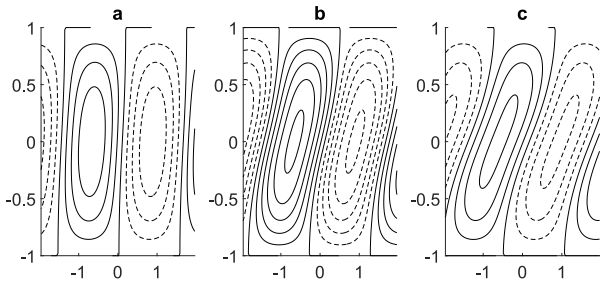

Figure 8. Streamwise fluctuations are shown over the spanwise direction x_3 and wall-normal direction x_2 for (a) $\beta = 2$, $Re_\alpha = 1$, $\omega_1 = -10.1588$i, (b) $\beta = 2$, $Re_\alpha = 5$, $\omega_1 = -2.0508$i and (c) $\beta = 2$, $Re_\alpha = 10$, $\omega_1 = -1.0522$i as pairs of vortices. Solid lines represent fluctuations with a positive sign, while dashed lines represnent fluctuations with a negative sign.

CONCLUSION AND OUTLOOK

In this work the resolvent analysis was used in order to investigate the linear amplification mechanisms leading to coherent structures in laminar plane Couette flow with emphasis on the distinguished asymptotic case with high Reynolds numbers $Re \to \infty$ and small streamwise wavenumbers $\alpha \to 0$, with $Re_\alpha = Re \cdot \alpha = O(1)$.

Through a SVD decomposition of the input-output system (14) the most amplified structures and the energy of the system were analysed with using the knowledge of the laminar base velocity profile only. The influence of the streamwise and spanwise wavenumbers α and β, as well as the Reynolds number Re on the first singular value σ_1, which represents the energy of the system, were investigated. The influence of Re_α on the streamwise velocity fluctuation was investigated, where it could be seen that an increase of Re_α lead to stronger inclinations of the streamwise velocity fluctuation within the wall-normal and spanwise plane due to the Orr-mechanism. Additionally the applicability of the distinguished limit with $Re_\alpha = Re \cdot \alpha = O(1)$ for the linear stability theory was examined, where the eigenvalues of the Orr-Sommerfeld equation could be obtained only depending on Re_α, while analytical expressions for the eigenfunctions could be obtained using both the Orr-Sommerfeld and Squire equation. It could be seen that α only acts as a magnitude amplifier for both the wall-normal and the spanwise velocity fluctuation fluctuation $\tilde{u}'_2$ and $\tilde{u}'_3$, while the wall-normal vorticity $\tilde{\eta}'_2$ and thus the streamwise fluctuation $\tilde{u}'_1$ are only dependent on Re_α for the distinguished limit with high Reynolds numbers $Re \to \infty$ and small streamwise wavenumbers $\alpha \to 0$. Once again an increase of Re_α lead to inclined structures within the wall-normal and spanwise plane. The eigenfunctions obtained from the linear stability theory and the response modes from the resolvent analysis were compared, where it could be seen that in both cases the most energy can be found in the streamwise direction, whereas the amplitudes of the velocity fluctuations in wall-normal and spanwise direction are in the order of $O(\alpha)$ smaller compared to the streamwise velocity fluctuations.

A first extension to this work is planned by also considering a turbulent mean velocity profile obtained from DNS data. Additionally the response of the resolvent system with frequencies close to the eigenvalues can be investigated in order to analyse possible pseudo-resonance phenomena. Furthermore various modifications, such as the plane Couette flow with wall-transpiration can be analysed in the future, where the influence of the wall-transpiration velocity on the stability of the coherent structures could be a focus of the analysis.

REFERENCES

Gustavsson, L. 1981 Energy growth of three-dimensional disturbances in plane poiseuille flow. *Journal of Fluid Mechanics* **224**, 241–260.

Hwang, Yongyun & Cossu, Carlo 2010*a* Amplification of coherent streaks in the turbulent couette flow: an input–output analysis at low reynolds number. *Journal of Fluid Mechanics* **643**, 333–348.

Hwang, Yongyun & Cossu, Carlo 2010*b* Linear non-normal energy amplification of harmonic and stochastic forcing in the turbulent channel flow. *Journal of Fluid Mechanics* **664**, 51–73.

Schmid, Peter & Henningson, Dan 2001 *Stability and Transition in Shear Flows*, , vol. 142. Springer.

Weideman, J. A. & Reddy, S. C. 2000 A matlab differentiation matrix suite. *ACM Trans. Math. Softw.* **26** (4), 465–519.

Yalcin, Alparslan, Turkac, Y. & Oberlack, Martin 2021 On the temporal linear stability of the asymptotic suction boundary layer. *Physics of Fluids* **33**, 054111.